

Inkjet Printing Patterns of Highly Conductive Pristine Graphene on Flexible Substrates

Yahui Gao,^{†,‡} Wen Shi,[†] Wucong Wang,[†] Yuanpeng Leng,[†] and Yaping Zhao^{*,†}

[†]School of Chemistry and Chemical Engineering, Shanghai Jiao Tong University, 800 Dong Chuan Road, Shanghai 200240, China

[‡]Department of Environmental Engineering and Chemistry, Luoyang Institute of Science and Technology, 90 Wang Cheng Road, Luoyang 471023, China

Supporting Information

ABSTRACT: Highly conductive pristine graphene electrodes were fabricated by inkjet printing using ethyl cellulose-stabilized ink prepared from pristine graphene. Pristine graphene was generated by exfoliation from graphite using ultrasound-assisted supercritical CO₂. The ink, at concentrations up to 1 mg/mL, was stable for more than 9 months and had compatible fluidic characteristics for efficient and reliable inkjet printing. The inkjet printing patterns of the graphene on diverse substrates were uniform and continuous. After 30 printing passes and annealing at 300 °C for 30 min, the printed films developed a high conductivity of 9.24 × 10³ S/m. The resistivity of the printed electrodes on the flexible substrates increased by less than 5% after 1000 bending cycles and by 5.3% under a folding angle of 180°. The presented exfoliated pristine graphene and the corresponding efficient methods for formulating the ink and fabricating conductive electrodes are expected to have high potential in applications involving graphene-based flexible electronic devices.

1. INTRODUCTION

Inkjet printing is one of the most promising techniques for the low-cost and large-area fabrication of flexible electronics, such as electronic displays,^{1,2} field-effect transistors (FETs),³ solar cells,^{4,5} sensors,⁶ and transparent electrodes.⁷ Its significant advantages include few process steps, digital and additive patterning, low material waste, low temperature, and compatibility with various substrates.⁵ Graphene can be a good ink for inkjet printing because of its high conductivity and chemical stability.^{8–10} Reduced graphene oxide (RGO) ink was developed for fabricating a series of flexible devices by inkjet printing.^{11–17} However, the poor electrical properties of RGO limit the applications of these devices. To overcome the disadvantages of RGO-formulated ink, pristine graphene ink was developed, which has the high electrical conductivity characteristic to graphene. Torrisi et al.¹⁸ and Han et al.¹⁹ used pristine graphene prepared by the liquid-phase exfoliation (LEP) of graphite in *N*-methylpyrrolidone (NMP) to print thin film transistors (TFTs). However, a low graphene concentration (0.11 mg/mL) reduced the efficiency of the inkjet printing, and the residual solvent in the printed electronics also impaired the electrical conductivity. Li et al.^{20,21} prepared pristine graphene–terpineol ink using LEP and a solvent exchange technique. However, the process was time-consuming. Moreover, the solvents used, such as *N,N*-dimethylformamide (DMF) and NMP, were toxic and difficult to completely remove from the substrates. Hersam and co-workers^{22,23} prepared pristine graphene by exfoliation in ethanol instead of a toxic solvent and made ethyl cellulose- (EC-) stabilized graphene ink. The conductivity of their inkjet-printed graphene patterns was 4 mΩ·cm. However, this method involved the repeated and complicated process of salt flocculation and redispersion in solvent to obtain a graphene/EC powder, which limits its application. Therefore, it is highly desirable to develop a simple and practical method for formulating pristine graphene ink without using toxic and high-boiling-point solvents.

The pristine graphene ink, having a high concentration and stability, could then be used in inkjet printing to fabricate high-conductivity electrodes in graphene-printed patterns.

The purpose of this work was to formulate a pristine graphene ink with high concentration and stability and to fabricate electrodes with high electrical conductivity. The pristine graphene was first prepared by exfoliating graphite using ultrasound-assisted supercritical CO₂. Then, the graphene ink was formulated using cyclohexanone and EC as a solvent and a stabilizing agent, respectively. Finally, the formulated ink was used to print electrodes using a Dimatix Materials Printer. The stability of the ink and the resistivity of the electrodes were investigated.

2. EXPERIMENTAL SECTION

2.1. Materials and Reagents. Graphite powder was purchased from Sinopharm Chemical Reagent Co., Ltd. (Beijing, China) (10–50-μm particle size). Carbon dioxide (99.9%) was obtained from Shanghai High-Tech Co., Ltd. (Shanghai, China). Cyclohexanone (99.5%), ethylene glycol (EG, 99.0%), hexamethyldisilazane (HMDS, 97.0%), and ethyl cellulose (EC; 8–10 cP viscosity for 5% (w/v) in 1:4 ethanol/toluene, 43–50% ethoxy) were purchased from Sinopharm Chemical Reagent Co., Ltd. (Beijing, China). All reagents were used as received.

2.2. Preparation of Pristine Graphene Ink and Its Properties. **2.2.1. Ink Preparation.** The ink studied in this work consisted of pristine graphene flakes, EC, and cyclohexanone. Pristine graphene sheets were prepared by exfoliating graphite using ultrasound-assisted supercritical CO₂. The procedure was reported in our earlier publication²⁴ and is also described in

Received: July 7, 2014

Revised: September 30, 2014

Accepted: October 1, 2014

Published: October 1, 2014

Supporting Information section 1; characterization methods of exfoliated graphene sheets are discussed in Supporting Information section 2.

The exfoliated pristine graphene sheets were mixed in a beaker with 30 mL of 0.1% (w/v) EC/cyclohexanone solution. The resultant suspension was dispersed in an ultrasonic bath (40 W) for 30 min to improve the graphene distribution in the EC. Large flakes of the suspension were removed by centrifugation

at 10000 rp (approximately 10250g) for 30 min (TG16-II, Changsha Pingfan Instrument and Meter Co., Ltd., Changsha, China). The graphene concentration was calculated using the Lambert–Beer law: $A/l = \alpha_{660}C$, where l is the cell length and the absorption coefficient²⁵ is $\alpha_{660} = 2460 \text{ L g}^{-1} \text{ m}^{-1}$. The absorbance of the as-prepared graphene suspension was measured by a UV-vis spectrophotometer (PC 756, Shanghai Spectrum Instruments Co., Ltd., Shanghai, China) at $\lambda = 660 \text{ nm}$. The graphene concentration of the ink was adjusted to 1.0 mg/mL (0.72 wt % solids content).

2.2.2. Measurement of Physical Properties of the Ink. The viscosity of the prepared ink was measured on an Ubbelohde viscosity meter with a 0.5–0.6-mm capillary inner diameter (Shanghai Liangjing Glass Instrument Co., Shanghai, China). The surface tension of the ink was determined by a plate method using a fully automatic surface tension meter (K100, Krüss GmbH Co., Hamburg, Germany).

To investigate their thermal stability, thermal gravimetric analysis (TGA) of EC and the ink composite material was performed using a TGA 7 thermal gravimetric analyzer (Perkin-Elmer, Inc., Wellesley, MA) at a heating rate of 10 °C/min in air.

2.3. Fabrication and Characterization of Graphene Patterns.

Inkjet printing patterns of the pristine graphene were created using a piezoelectric Dimatix Materials Printer (DMP2800, Dimatix-Fujifilm Inc.) equipped with a cartridge (DMC-11610) designed for a 10 pL nominal drop volume. The prepared ink was syringe-injected into a cleaned cartridge. Before printing, the operating parameters of the jetting droplets from each nozzle were optimized to minimize tails and satellites.²⁶ Patterns were then printed onto various substrates,

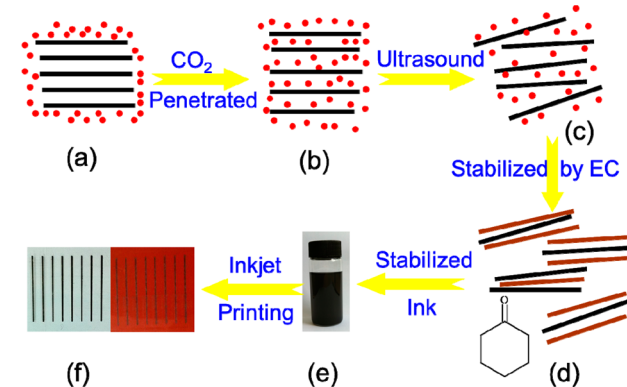


Figure 1. Schematic illustration of the preparation process of pristine graphene ink and its printed electrodes. (a) Layered graphite was immersed in supercritical CO_2 . (b) CO_2 molecules penetrated in the interlayer of graphite, (c) forming single- or few-layer-thick graphene sheets. (d) Graphene sheets were stabilized by EC in cyclohexanone and (e) formed stable graphene ink. (f) Graphene electrodes were printed on PET and PI substrates.

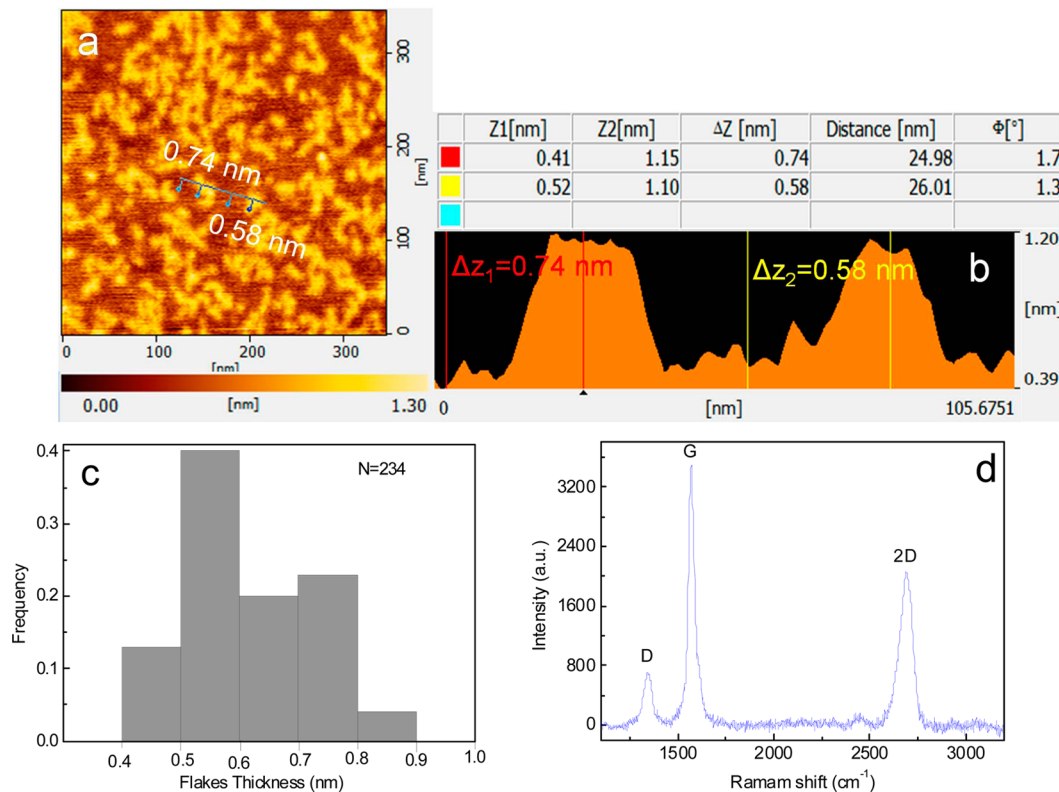


Figure 2. Characterization of graphene sheets. (a) Representative AFM image ($350 \text{ nm} \times 350 \text{ nm}$) of the graphene sheets. (b) Cross-sectional height profile along the lines shown in panel a. (c) Histogram of sheet thickness derived from height measurements of approximately 234 sheets in AFM images. (d) Raman spectrum of graphene sheets deposited on Si/SiO_2 (300 nm).

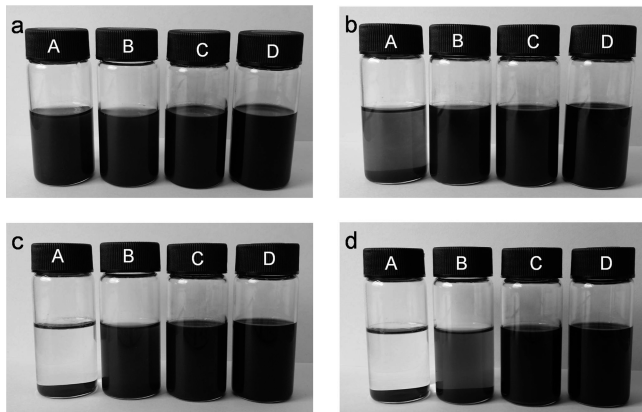


Figure 3. Photographs of the different ink formulations monitored over time. Images were taken (a) immediately after preparation, (b) after 24 h, (c) after 1 week, and (d) after 1 month. The EC concentrations in cyclohexanone (% w/v) were 0.0 (sample A), 0.01 (sample B), 0.05 (sample C), and 0.1 (sample D).

including normal printing paper, glass slides, poly(ethylene terephthalate) (PET, 150 μm), and polyimide (PI, DuPont Kapton 125 μm). The printed PI films (5 mm \times 10 mm) were annealed in a high-temperature furnace (NBD-01200X IC, Nobody Materials Science and Technology Co., Ltd, Henan, China) with systematic variations in the annealing time and temperature.

To investigate the continuity and uniformity of the printed patterns with various printing passes on substrates, a Hitachi S-4800 field-emission scanning electron microscope, operated at 10 kV and 9 μA , was used to characterize the morphology of the printed patterns.

The resistivity of the printed patterns was measured using a four-point probe resistivity measurement system with silver paint electrodes (SX1944, Suzhou Baisheng Technology Co., Ltd., Suzhou, China), employing the appropriate geometric correction factors. The film thickness was measured by profilometry (D120 Stylus Surface Profiler, KLA-Tencor Co., North Wales, PA).

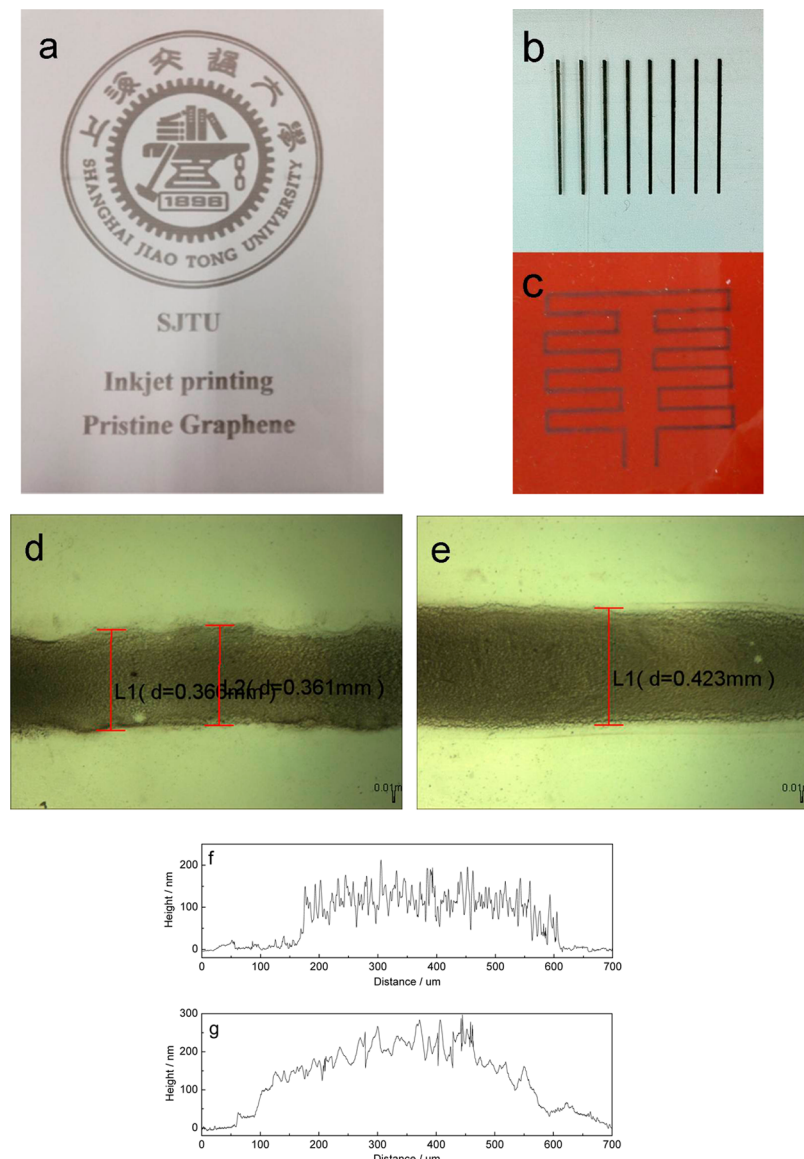


Figure 4. Inkjet-printed graphene patterns on various substrates: (a) normal paper; (b) PET; (c) PI; (d,e) glass slides at 30 and 40 printing passes, respectively; and (f,g) cross-sectional profiles of printed electrodes in panels d and e, respectively.

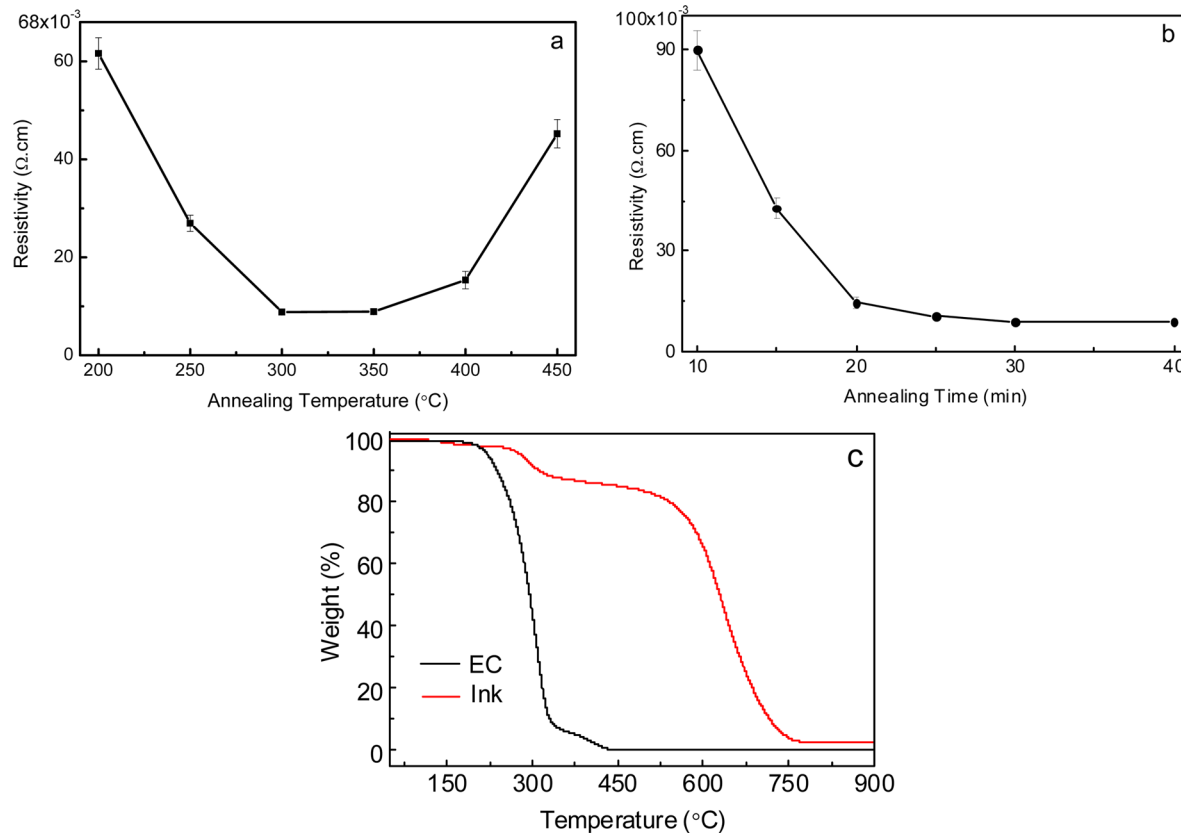


Figure 5. Effects of annealing time and temperature on the resistivity of the printed patterns; TGA curves of pure EC and ink powder. (a,b) Electrical resistivity of printed patterns plotted against (a) annealing temperature for a fixed annealing time of 30 min and (b) annealing time at a fixed annealing temperature of 300 °C. (c) TGA curves of pure EC and ink material powder as weight percentage vs temperature.

3. RESULTS AND DISCUSSION

3.1. Exfoliation of Graphene, Formulation of Ink, and Fabrication of Electrodes. The pristine graphene was prepared by an ultrasound-assisted supercritical CO_2 technique as shown in Figure 1a–c. When the graphite was immersed in supercritical CO_2 (Figure 1a), CO_2 molecules, because of their high diffusivity, small molecular size, and low interfacial tension and viscosity, diffused into the interstitial space between graphene layers (Figure 1b). As the CO_2 molecules accumulated in the graphitic interlayer, the distance between the layers expanded. Under ultrasonic vibration, CO_2 molecules and graphite absorb more energy from collapsing cavitation bubbles, resulting in the exfoliation of graphite into single- or few-layer-thick graphene sheets (Figure 1c).

After ultrasound-assisted exfoliation, the ink was prepared by directly spraying the exfoliated graphene sheets into an EC/cyclohexanone solution from the reactor, as shown in Figure 1d,e. EC acted as a stabilizing agent. The ink was stable for long periods.

Finally, graphene electrodes were printed on the substrates by inkjet printing using a piezoelectric Dimatix Materials Printer (Figure 1f).

3.1.1. Characterization of Graphene Sheets. The number of layers of exfoliated graphene and any defects will affect the quality of the electrodes. Therefore, we characterized the exfoliated graphene using atomic force microscopy (AFM) and Raman spectroscopy. As shown in Figure 2a–c, the AFM image of the exfoliated graphene sheets and the statistical histogram of their thickness indicated that the average thickness and lateral size were less than 1 nm and approximately 30–100 nm,

respectively. This observed thickness was less (i.e., these layers were thinner) than those reported in prior work.^{21,22} This suggests that there were only a few layers of graphene sheets (i.e., <5 layers), which was confirmed by the shapes and intensities of the 2D peaks in the Raman spectrum shown in Figure 2d.^{27,28} Furthermore, the graphene sheets were defect-free, which can be demonstrated by the intensity ratio of the D band (approximately 1343 cm^{-1}) to the G band (approximately 1571 cm^{-1}), I_D/I_G , of approximately 0.2, which is lower than the 0.5–0.7 values reported by Li et al.^{20,21} Moreover, it was demonstrated in our previous work²⁴ that a pristine graphene sheet can maintain crystallinity in a hexagonally symmetric structure without oxygen-containing groups or any other groups being introduced during the exfoliation process.

3.1.2. Stability of the Ink. Ink stability is an important index for inkjet printing. We examined the influence of storage time and concentration of EC (as the stabilizing polymer) in cyclohexanone solvent on the stability of the ink. As shown in Figure 3, the stability of the ink increased with the EC concentration. For sample A, almost all of the graphene sheets deposited and sedimented at the bottom of the vial after 24 h. For samples B and C, small amounts of settling were observed after 1 week and 1 month, respectively. However, for sample D, even after 9 months, no graphene sheets were observed to settle at the bottom; this suggests that the ink is very stable. This stability is mainly because the strong interactions caused by hydrophobic interactions between EC and the graphene sheets counter the van der Waals forces between the graphene flakes, thereby inhibiting the aggregation of the graphene.²¹ Therefore, the formulation of graphene ink used a concentration of 0.1% (w/v) EC in cyclohexanone.

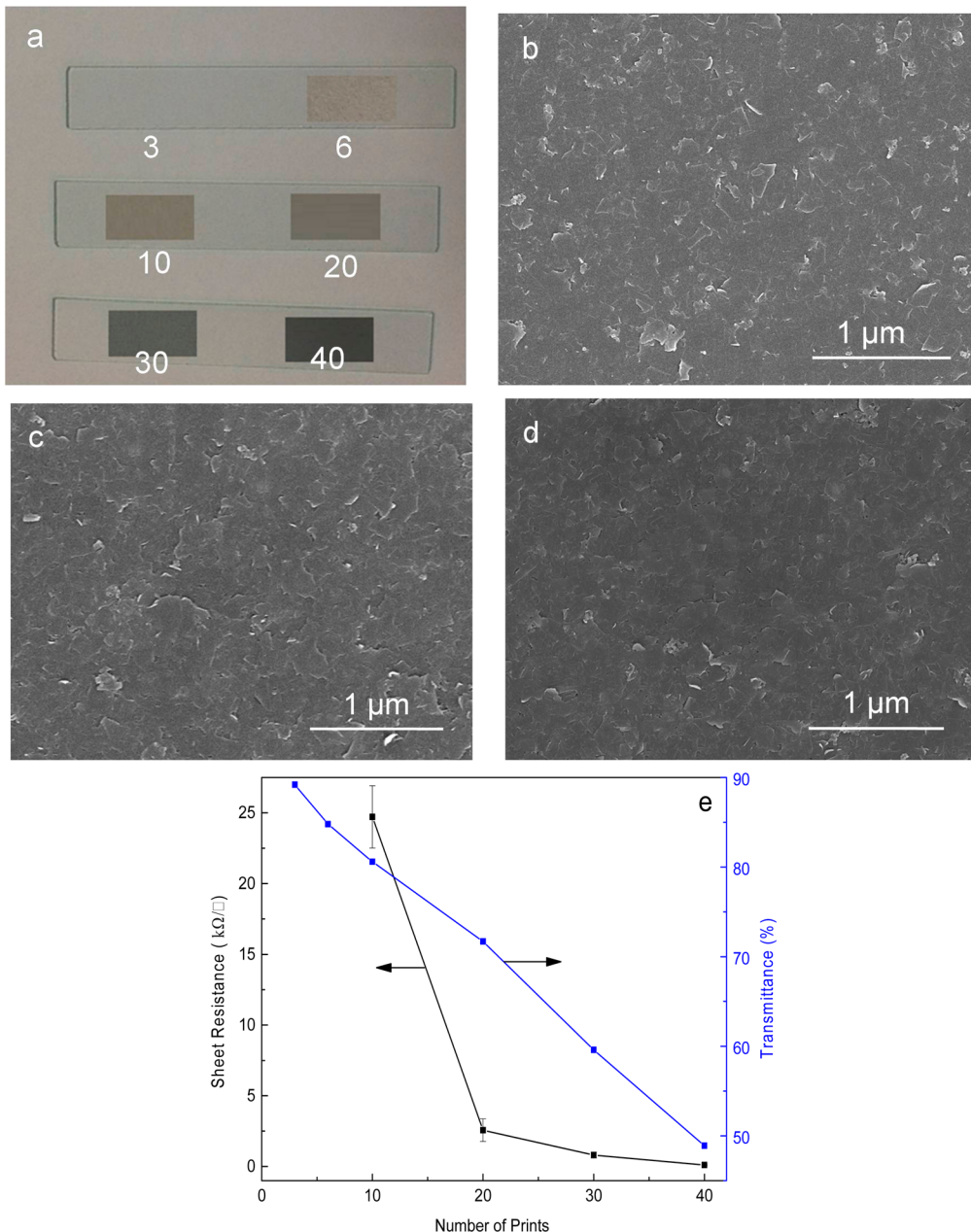


Figure 6. Inkjet-printed graphene conductive patterns. (a) Photograph of the printed patterns after various printing passes (from 3 to 40). (b–d) Scanning electron microscopy (SEM) images of the printed patterns after 10, 30, and 40 printing passes, respectively. (e) Sheet resistance and transmittance (at $\lambda = 550$ nm) of the printed patterns with increasing numbers of printing passes. Transmittance spectra of all six patterns in panel a are shown in Figure S2 in Supporting Information section 5.

3.1.3. Inkjet-Printed Electrodes. To generate the uniform droplets in the process of inkjet printing, the fluidic properties of ink, including viscosity, η (cP), and surface tension, γ (mN/m), require careful optimization.^{26,29} In general, these parameters and other factors, such as nozzle diameter d (μm), density ρ (g/cm^3), and drop velocity v (m/s), can be arranged into dimensionless figures of merit (FOM), such as the Reynolds number ($Re = dv\rho/\eta$), Weber number ($We = v^2\rho d/\gamma$), and Ohnesorge number [$Oh = We^{1/2}/Re = \eta/(\gamma pd)^{1/2}$]. Jang et al.²⁶ suggested using $Z = 1/Oh$ as an appropriate FOM to characterize drop formation. A Z range between 1 and 14 is required to achieve a stable drop. Therefore, before printing, suitable amounts of EG were added to alter the viscosity and surface tension to make the ink compatible with inkjet printing. When the volume ratio of cyclohexanone and

EG was 4:1, the graphene ink had a surface tension of 33.45 mN/m and a viscosity of 10 cP. Given these parameters and a nozzle diameter of 50 μm , we obtained a Z value of $Z = (\gamma\rho d)^{1/2}/\eta = 4.3$ that was within the suitable range for printing. The drop formation video captured by the Drop Watcher system of the printer demonstrates that the inks provided well-directed and constant jetting from all nozzles at a stable velocity (see Supporting Information section 3, Video 1).

In addition to the properties of ink, the surface properties of substrates determine the optimal drop pitch and thereby affect the printing quality.^{26,29} Therefore, the wetting properties of the ink on various substrates such as PET, PI, and glass slides must be optimized to achieve the proper morphology of the printed features. To satisfy this requirement, we pretreated the

substrates with hexamethyldisilazane (HMDS; Supporting Information section 4) and evaluated the wetting properties of the substrates based on the values of their contact angles. The contact angles of the HMDS-treated PET, PI, and glass slide were approximately 77.9°, 77.2°, and 77.8°, respectively (Supporting Information section 4, Figure S1). As shown in Figure 4a–c, the patterns and electrodes printed on normal printing paper and on HMDS-treated PET, PI, and glass slides were continuous and highly uniform, confirming the printing reliability and efficiency. Furthermore, the electrodes maintained excellent uniformity even at 30 and 40 printing passes, as shown by digital micrographs (Figure 4d,e), and their average cross-sectional profiles of printed lines (Figure 4f,g) were 150 ± 35 and 200 ± 20 nm, respectively. It is worth noticing that no coffee-ring effect^{12,18} observed in the printed electrodes. When the ink drop deposited onto the HMDS-coated substrates, graphene flakes were likely confined into smaller areas because of their greater hydrophobicity. Additionally, the presence of silane on HMDS-treated substrates might promote the adhesion of graphene to the substrate.¹⁸ Therefore, more uniform graphene flakes with a regular distribution formed without the coffee-ring effect.

3.2. Resistivity of Printed Patterns. **3.2.1. Influence of Annealing Conditions on Resistivity.** The annealing temperature and time were found to have significant influences on the electrical behavior of the printed patterns. As shown in Figure 5a, the resistivity decreased from 61.6 to $10.82 \text{ m}\Omega\cdot\text{cm}$ as the annealing temperature was increased from 200 to 350 °C. This result can be attributed to the volatilization of the residual solvent and the thermal decomposition of EC (Figure 5c) into aromatic compounds.³⁰ The decomposition also resulted in a $\pi-\pi$ bond stack between the EC residues and the graphene flakes; in turn, this provided efficient charge transport and

decreased the resistivity through the graphene network.²² However, at temperatures above 350 °C, the resistivity increased. This behavior can be attributed to two causes. Graphene was oxidized above 400 °C, and the EC residue in the graphene network was removed. Annealing time had a similar influence. As shown in Figure 5b, the resistivity sharply decreased from 89.9 to $10.82 \text{ m}\Omega\cdot\text{cm}$ and gradually reached a steady state as the annealing time was increased from 10 to 30 min. This can be explained by the fact that the amount of aromatic compounds in the graphene network increased with increasing annealing time and the concentration remained steady after 30 min.

3.2.2. Transmittance and Electrical Conductivity. To investigate the transmittance and electrical performance of the printed patterns, centimeter-scale graphene films ($20 \text{ mm} \times 10 \text{ mm}$) at various numbers of passes were printed on HMDS-treated glass slides substrates. As shown in Figure 6a, the printed films became darker as the number of printing passes increased from 3 to 40. The continuity of the printed patterns improved as the number of printing passes increased from 10 to 40, as shown in Figure 6b–d. Highly uniform and continuous patterns were obtained after 30 printing passes. However, the transmittance of the patterns reduced as the number of printing passes increased. As shown in Figure 6e, the sheet resistance of the patterns decreased as the number of printing passes increased, reaching a relatively stable and low value after 30 printing passes; the transmittance continually decreased. After 30 printing passes, the transmittance was 60% (at $\lambda = 550 \text{ nm}$), and the sheet resistance was $0.81 \pm 0.2 \text{ k}\Omega/\square$. The lower sheet resistances of the printed patterns can be attributed to the high quality of the pristine graphene sheets and good junctions in the graphene network.

3.2.3. Flexibility and Electrical Conductivity. To evaluate the flexibility of the printed electrodes, lines (with a length of 25 mm) that had been printed on the PI substrates (Figure 7a)

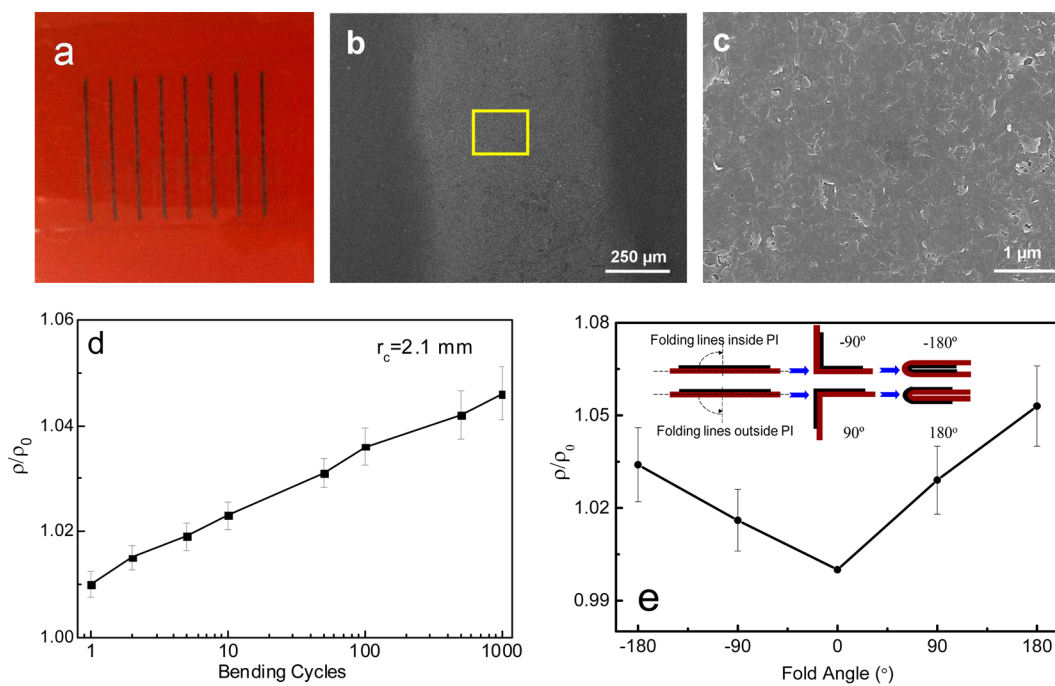


Figure 7. Flexibility assessment of printed graphene electrodes on PI substrates. (a) Photograph of printed electrodes of 25-mm length on a PI substrate. (b) SEM image of printed lines. (c) Higher-magnification SEM image of the highlighted area (yellow box) from panel b. (d) Relative resistivity of the original graphene electrodes and after repeated bending. (e) Relative resistivity of the original graphene electrode and after folding under various folding angles. Inset: Schematic diagrams of the folding angles. Data collected from eight lines; error bars represent one standard deviation.

and annealed at 300 °C for 30 min were subjected to deformation through bending cycles and various folding angles. SEM images (Figure 7b,c) show that the printed electrodes were continuous and uniform and formed good junctions between flakes. The electrical resistivity of the graphene electrodes increased by only 3.6% and 4.6% after 100 and 1000 bending cycles, respectively, as shown in Figure 7d. No cracks were observed in the electrodes. Figure 7e displays the relative resistivity of the electrodes under various folding angles. Slight increases in resistivity were observed: 1.6% and 3.4% under -90° and -180° folding angles, respectively, and 2.9% and 5.3% under 90° and 180° folding angles, respectively. In the folded state, cracking was observed in the substrate, which suggests that a small conductivity loss was caused by a limitation of the substrate rather than the printed patterns. These results indicate that inkjet printing of the formulated ink can fabricate flexible and foldable electrodes with high conductivity.

4. CONCLUSIONS

Pristine graphene ink was formulated and used to prepare electrodes with high electrical conductivity. The pristine graphene sheets in the formulation ink were less than 1 nm thick and 30–100 nm laterally. The graphene ink, when adequately dispersed in EC, was stable for more than 9 months. The sheet resistance of the printed films after 30 printing passes was only $0.81 \pm 0.2 \text{ k}\Omega/\square$, and the films had a transmittance of approximately 60% after being annealed at 300 °C for 30 min. The electrical resistivity of the printed electrodes on flexible substrates increased only slightly despite 1000 bending or folding cycles. The formulated pristine graphene ink is expected to have significant potential applications in fabricating flexible electric devices.

■ ASSOCIATED CONTENT

S Supporting Information

Detailed preparation procedure of pristine graphene and ink, AFM and Raman characterization, video of jetting ink, surface modification of substrates and contact angle images, transmittance spectra of printed graphene patterns. This material is available free of charge via the Internet at <http://pubs.acs.org>.

■ AUTHOR INFORMATION

Corresponding Author

*Tel.: +86-021-54743274. Fax: +86-021-54741297. E-mail: ypzhao@sjtu.edu.cn.

Notes

The authors declare no competing financial interest.

■ ACKNOWLEDGMENTS

We are thankful to the group of Professor Xiaojun Guo of the School of Electronic Information and Electrical Engineering of SJTU for access to their inkjet printer and surface profiler and Ms. Huiqin Li of the Instrumental Analysis Center of SJTU for AFM analysis.

■ REFERENCES

- Wood, V.; Panzer, M. J.; Chen, J.; Bradley, M. S.; Halpert, J. E.; Bawendi, M. G.; Bulović, V. Inkjet-Printed Quantum Dot–Polymer Composites for Full-Color AC-Driven Displays. *Adv. Mater.* **2009**, *21*, 2151–2155.
- Shen, W.; Zhang, X.; Huang, Q.; Xu, Q.; Song, W. Preparation of solid silver nanoparticles for inkjet printed flexible electronics with high conductivity. *Nanoscale* **2014**, *6*, 1622–1628.
- Liu, R.; Shen, F.; Ding, H.; Lin, J.; Gu, W.; Cui, Z.; Zhang, T. All-carbon-based field effect transistors fabricated by aerosol jet printing on flexible substrates. *J. Micromech. Microeng.* **2013**, *23*, 065027–065033.
- Gaikwad, A. M.; Whiting, G. L.; Steingart, D. A.; Arias, A. C. Highly Flexible, Printed Alkaline Batteries Based on Mesh-Embedded Electrodes. *Adv. Mater.* **2011**, *23*, 3251–3255.
- Singh, M.; Haverinen, H. M.; Dhagat, P.; Jabbour, G. E. Inkjet printing—Process and its applications. *Adv. Mater.* **2010**, *22*, 673–685.
- Mabrook, M. F.; Pearson, C.; Jombert, A. S.; Zeze, D. A.; Petty, M. C. The morphology, electrical conductivity and vapour sensing ability of inkjet-printed thin films of single-wall carbon nanotubes. *Carbon* **2009**, *47*, 752–757.
- Kwon, O.-S.; Kim, H.; Ko, H.; Lee, J.; Lee, B.; Jung, C.-H.; Choi, J.-H.; Shin, K. Fabrication and characterization of inkjet-printed carbon nanotube electrode patterns on paper. *Carbon* **2013**, *58*, 116–127.
- Nair, R. R.; Blake, P.; Grigorenko, A. N.; Novoselov, K. S.; Booth, T. J.; Stauber, T.; Peres, N. M. R.; Geim, A. K. Fine structure constant defines visual transparency of graphene. *Science* **2008**, *320*, 1308–1308.
- Castro Neto, A. H.; Guinea, F.; Peres, N. M. R.; Novoselov, K. S.; Geim, A. K. The electronic properties of graphene. *Rev. Mod. Phys.* **2009**, *81*, 109–162.
- Novoselov, K. S.; Fal'ko, V. I.; Colombo, L.; Gellert, P. R.; Schwab, M. G.; Kim, K. A Roadmap for Graphene. *Nature* **2012**, *490*, 192–200.
- Dua, V.; Surwade, S. P.; Ammu, S.; Agnihotra, S. R.; Jain, S.; Roberts, K. E.; Park, S.; Ruoff, R. S.; Manohar, S. K. All-Organic Vapor Sensor Using Inkjet-Printed Reduced Graphene Oxide. *Angew. Chem., Int. Ed.* **2010**, *49*, 2154–2157.
- Huang, L.; Huang, Y.; Liang, J.; Wan, X.; Chen, Y. Graphene-Based Conducting Inks for Direct Inkjet Printing of Flexible Conductive Patterns and Their Applications in Electric Circuits and Chemical Sensors. *Nano. Res.* **2011**, *4*, 675–684.
- Sinar, D.; Knopf, G. K.; Nikumb, S. Graphene-based inkjet printing of flexible bioelectronic circuits and sensors. *Proc. SPIE* **2013**, *8612*, 861204–861204.
- Lee, C.-L.; Chen, C.-H.; Chen, C.-W. Graphene nanosheets as ink particles for inkjet printing on flexible board. *J. Chem. Eng.* **2013**, *230*, 296–302.
- Wang, X.; Zhi, L.; Müllen, K. Transparent, Conductive Graphene Electrodes for Dye-Sensitized Solar Cells. *Nano Lett.* **2008**, *8*, 323–327.
- Kong, D.; Le, L. T.; Li, Y.; Zunino, J. L.; Lee, W. Temperature-Dependent Electrical Properties of Graphene Inkjet-Printed on Flexible Materials. *Langmuir* **2012**, *28*, 13467–13472.
- Le, L. T.; Ervin, M. H.; Qiu, H.; Fuchs, B. E.; Lee, W. Y. Graphene supercapacitor electrodes fabricated by inkjet printing and thermal reduction of graphene oxide. *Electrochim. Commun.* **2011**, *13*, 355–358.
- Torrisi, F.; Hasan, T.; Wu, W.; Sun, Z.; Lombardo, A.; Kulmala, T. S.; Hsieh, G.-W.; Jung, S.; Bonaccorso, F.; Paul, P. J. Inkjet-Printed Graphene Electronics. *ACS Nano* **2012**, *6*, 2992–3006.
- Han, X.; Chen, Y.; Zhu, H.; Preston, C.; Wan, J.; Fang, Z.; Hu, L. Scalable, printable, surfactant-free graphene ink directly from graphite. *Nanotechnology* **2013**, *24*, 205304–205311.
- Li, J.; Ye, F.; Vaziri, S.; Muhammed, M.; Lemme, M. C.; Östling, M. Efficient Inkjet Printing of Graphene. *Adv. Mater.* **2013**, *19*, 3973–3978.
- Li, J.; Ye, F.; Vaziri, S.; Muhammed, M.; Lemme, M. C.; Östling, M. A simple route towards high-concentration surfactant-free graphene dispersions. *Carbon* **2012**, *50*, 3092–3116.
- Secor, E. B.; Prabhmirashi, P. L.; Puntambekar, K.; Geier, M. L.; Hersam, M. C. Inkjet Printing of High Conductivity, Flexible Graphene Patterns. *J. Phys. Chem. Lett.* **2013**, *4*, 1347–1351.
- Liang, Y. T.; Hersam, M. C. Highly Concentrated Graphene Solutions via Polymer Enhanced Solvent Exfoliation and Iterative Solvent Exchange. *J. Am. Chem. Soc.* **2010**, *132*, 17661–17663.

- (24) Gao, Y. H.; Shi, W.; Wang, W. C.; Wang, Y.; Zhao, Y. P.; Lei, Z. H.; Miao, R. R. Ultrasonic-Assisted Production of Graphene with High Yield in Supercritical CO₂ and Its High Electrical Conductivity Film. *Ind. Eng. Chem. Res.* **2014**, *53*, 2839–2845.
- (25) Hernandez, Y.; Nicolosi, V.; Lotya, M.; Blighe, F. M.; Sun, Z.; De, S.; McGovern, I. T.; Holland, B.; Byrne, M.; Gun'Ko, Y. K.; Boland, J. J.; Niraj, P.; Duesberg, G.; Krishnamurthy, S.; Goodhue, R.; Hutchison, J.; Scardaci, V.; Ferrari, A. C.; Coleman, J. N. High-yield production of graphene by liquid-phase exfoliation of graphite. *Nat. Nanotechnol.* **2008**, *3*, 563–568.
- (26) Jang, D.; Kim, D.; Moon, J. Influence of Fluid Physical Properties on Ink-Jet Printability. *Langmuir* **2009**, *25*, 2629–2635.
- (27) Ferrari, A. C. Raman spectroscopy of graphene and graphite: Disorder, electron–phononcoupling, doping and nonadiabatic effects. *Solid State Commun.* **2007**, *143*, 47–57.
- (28) Rangappa, D.; Sone, K.; Wang, M. S.; Gautam, U. K.; Golberg, D.; Itoh, H.; Ichihara, M.; Honma, I. Rapid and direct conversion of graphite crystals into high-yielding, good-quality graphene by supercritical fluid exfoliation. *Chem.—Eur. J.* **2010**, *16*, 6488–6494.
- (29) Cummins, G.; Desmulliez, M. P.Y. Inkjet printing of conductive materials: A review. *Circuit World* **2012**, *38*, 193–213.
- (30) Keiluweit, M.; Nico, P. S.; Johnson, M. G.; Kleber, M. Dynamic Molecular Structure of Plant Biomass-Derived Black Carbon (Biochar). *Environ. Sci. Technol.* **2010**, *44*, 1247–1253.